Figure 4a and its projection into two dimensions (Fig. 4b) show the results of our simulations in Cu where cross-slip/double cross-slip takes place and irradiation-induced SFT defects are absorbed by sweeping dislocations based on the criterion discussed above. Figure 4 shows localization of plastic flow in defect-free channels. The channel width is approximately 200 nm with a channel spacing of 1,000 nm in agreement with experimental observations[1]. Examination of the simulation results reveals that the mechanism of channel formation can be described as follows. As dislocations propagate from a Frank–Read source, a screw dislocation segment may be pinned by the defects and eventually cross slip from its primary plane as the stress is increased. This is followed by double cross-slip of the segment, creating a new dislocation source on a parallel plane. This process continues with dislocation segments cross-slipping progressively from one glide plane to another, resulting in a set of parallel planes with active dislocations (the spacing between each pair of planes varies between 25 and 50 nm). Eventually, spreading of the band is limited by the interaction between segments of opposite sign that, in concert with the defects, exerts a backstress on those segments attempting to cross-slip. However, the process is continuous with dislocations being emitted from the same original single source, cross-slipping to adjacent planes and so on, resulting in a large local shear strain (about 100%) in the band. The spacing between the channels is a stochastic variable determined by the spatial distribution of dislocation sources. □

Received 23 February; accepted 30 June 2000.

1. Eyre, B. L. & Barlett, A. F. An electron microscope study of neutron irradiation damage on α-iron. *Phil. Mag.* **12,** 261–271 (1965).
2. Victoria, M. *et al.* The microstructure and associated tensile properties of irradiated fcc and bcc metals. *J. Nucl. Mater.* **276,** 114–122 (2000).
3. Odette, G. R. & Lucas, G. E. Recent progress in understanding reactor pressure vessel steel embrittlement. *Radiat. Effects Defects Solids* **144,** 189–231 (1998).
4. Bloom, E. E. The challenge of developing structural materials for fusion power systems. *J. Nucl. Mater.* **258–263,** 7–17 (1998).
5. Averback, R. S. & Diaz de la Rubia, T. in *Solid State Physics* Vol. 51 (eds Spaepen, F. *et al.* & Ehrenreich, H.) 281–402 (Academic, New York, 1998).
6. Dai, Y. & Victoria, M. Defect cluster structure and tensile properties of Cu single crystals irradiated with 600 MeV protons. *MRS Symp. Proc.* **439,** 319–324 (1997).
7. Friedel, J. *Dislocations* (Pergamon, Oxford, 1964).
8. Bement, A. L. Fundamental materials problems in nuclear reactors. In *Proc. 2nd Int. Conf. Strength of Metals Alloys* Vol. II, 693–728 (The American Society for Metals, 1970).
9. Trinkaus, H., Singh, B. N. & Foreman, A. J. E. Segregation of cascade induced interstitial loops at dislocations: possible effect on initiation of plastic deformation. *J. Nucl. Mater.* **251,** 172–187 (1997).
10. Singh, B. N., Foreman, A. J. E. & Trinkaus, H. Radiation hardening revisited: role of intracascade clustering. *J. Nucl. Mater.* **249,** 103–115 (1997).
11. Diaz de la Rubia, T. & Guinan, M. W. New mechanism of defect production in metals: A molecular-dynamics study of interstitial-dislocation-loop formation in high-energy displacement cascades. *Phys. Rev. Lett.* **66,** 2766–2769 (1991).
12. Foreman, A. J. E., Phythian, W. J. & English, C. A. The molecular dynamics simulation of irradiation damage cascades in copper using a many-body potential. *Phil. Mag. A* **66,** 671–695 (1992).
13. Wirth, B. D., Odette, G. R., Maroudas, D. & Lucas, G. E. *J. Nucl. Mater.* **244,** 185–194 (1997).
14. Osetsky, Y. N., Bacon, D. J. & Serra, A. Thermally activated glide of small dislocation loops in metals. *Phil. Mag. Lett.* **79,** 273–282 (1999).
15. Wirth, B. D., Bulatov, V. & Diaz de la Rubia, T. Atomistic simulation of stacking fault tetrahedra formation in Cu. *Proc. Int. Conf. Fusion Reactor Materials ICFRM-9, J. Nucl. Mater.* (in the press).
16. Heinisch, H. L. Computer simulation of high energy displacement cascades. *Radiat. Effects Defects Solids* **113,** 53–73 (1990).
17. Caturla, M. J. *et al.* Comparative study of radiation damage accumulation in Cu and Fe. *J. Nucl. Mater.* **276,** 13–21 (2000).
18. Soneda, N. & Diaz de la Rubia, T. Defect production, annealing kinetics and damage evolution in alpha-Fe: an atomic-scale computer simulation. *Phil. Mag. A* **78,** 995–1019 (1998).
19. Singh, B. N. & Zinkle, S. J. Defect accumulation in pure fcc metals in the transient regime: a review. *J. Nucl. Mater.* **206,** 212–229 (1993).
20. Baluc, N., Dai, Y. & Victoria, M. Plasticity and microstructure of irradiated Pd. *MRS Symp. Proc.* **540,** 555–560 (1999).
21. Baluc, N., Bailat, C., Luppo, M.-I., Schaublin, R. & Victoria, M. Comparison of the microstructure and tensile behavior irradiated fcc and bcc metals. *MRS Symp. Proc.* **540,** 539–548 (1999).
22. Zbib, H. M., Rhee, M. & Hirth, J. P. On plastic deformation and the dynamics of 3D dislocations. *Int. J. Mech. Sci.* **40,** 113–127 (1998).
23. Rhee, M., Zbib, H. M., Hirth, J. P., Huang, H. & Diaz de la Rubia, T. Models for long/short range interactions in 3D dislocation simulation. *Model. Simul. Mater. Sci. Eng.* **6,** 467–492 (1998).
24. Zbib, H. M., Diaz de la Rubia, T., Rhee, M. & Hirth, J. P. 3D dislocation dynamics: stress-strain behavior and hardening mechanisms in fcc and bcc metals. *J. Nucl. Mater.* **276,** 154–165 (2000).
25. Rhee, M., Lassila, D. H., Bulatov, V. V., Hshuing, L. & Diaz de la Rubia, T. Dislocation multiplication and the early stages of plastic deformation in bcc molybdenum: a dislocation dynamics numerical simulation. *Phys. Rev. Lett.* (submitted).
26. Khraishi, T. A., Zbib, H. M., Hirth, J. P. & Diaz de la Rubia, T. The stress field of a general circular Volterra dislocation loop: analytical and numerical approaches. *Phil. Mag. Lett.* **80,** 95–105 (2000).
27. Ghoniem, N. M., Singh, B. N., Sun, L. Z. & Diaz de la Rubia, T. Interaction and accumulation of glissile defect clusters near dislocations. *J. Nucl. Mater.* **276,** 166–177 (2000).
28. Rodney, D. & Martin, G. Dislocation pinning by small interstitial loops: a molecular dynamics study. *Phys. Rev. Lett.* **82,** 3272–3275 (1999).
29. Khraishi, T. A., Zbib, H. M., Diaz de la Rubia, T. & Victoria, M. Localized deformation and hardening in irradiated metals: 3D discrete dislocation dynamics simulations. *Acta Metall. Mater.* (submitted).

Acknowledgements

This work was performed in part under the auspices of the US Department of Energy by Lawrence Livermore National Laboratory. Work by M.V. was performed under a contract of the Swiss National Research Fund.

Correspondence and requests for materials should be addressed to T.D.R. (e-mail: delarubia@llnl.gov).

A stable argon compound

Leonid Khriachtchev, Mika Pettersson, Nino Runeberg, Jan Lundell & Markku Räsänen

Department of Chemistry, PO Box 55 (A.I.Virtasen aukio 1), FIN-00014 University of Helsinki, Finland

The noble gases have a particularly stable electronic configuration, comprising fully filled *s* and *p* valence orbitals. This makes these elements relatively non-reactive, and they exist at room temperature as monatomic gases. Pauling predicted[1] in 1933 that the heavier noble gases, whose valence electrons are screened by core electrons and thus less strongly bound, could form stable molecules. This prediction was verified in 1962 by the preparation of xenon hexafluoroplatinate, $XePtF_6$, the first compound to contain a noble-gas atom[2,3]. Since then, a range of different compounds containing radon, xenon and krypton have been theoretically anticipated and prepared[4–8]. Although the lighter noble gases neon, helium and argon are also expected to be reactive under suitable conditions[9,10], they remain the last three long-lived elements of the periodic table for which no stable compound is known. Here we report that the photolysis of hydrogen fluoride in a solid argon matrix leads to the formation of argon fluorohydride (HArF), which we have identified by probing the shift in the position of vibrational bands on isotopic substitution using infrared spectroscopy. Extensive *ab initio* calculations indicate that HArF is intrinsically stable, owing to significant ionic and covalent contributions to its bonding, thus confirming computational predictions[11–13] that argon should form a stable hydride species with properties similar to those of the analogous xenon and krypton compounds reported before[14–18].

We prepared hydrogen fluoride in an argon matrix by passing argon over an HF–pyridine polymer (Fluka) at room temperature, and condensing the mixture onto a CsI substrate kept at 7.5 K. The argon used was either ^{40}Ar (100%; AGA) or ^{36}Ar (99.5% isotopically enriched; ICON Services). By optimizing the experimental conditions, fairly monomeric samples of HF were obtained in the matrix (infrared bands corresponding to H–F stretching vibrations were found at $\nu_{HF} = 3{,}962$ and $3{,}954\ cm^{-1}$; $\nu_{DF} = 2{,}895\ cm^{-1}$), as evidenced by comparison with previous HF/Ar matrix-isolation studies[19]. A very high degree of deuteration ($> 90\%$) was achieved by passing the gaseous HF/Ar mixture through a volume containing small amounts of liquid deuterated sulphuric acid.

Photolysis of the HF was performed by illuminating the HF/Ar matrix (through a MgF_2 window) with a Kr vacuum-ultraviolet continuum discharge lamp (Opthos), which emitted in the spectral region of 127–160 nm wavelength. Typically, only a fraction ($< 30\%$) of HF dissociated when this light source was used, even

after extended periods of photolysis; this most probably indicates self-limitation of the photolysis due to formation of absorbing species[20], possibly involving charge-transfer excitation of impurity oxygen atoms.

After photolysis of the HF, three previously unknown bands appeared in the infrared spectra at about 1,969.5, 687.0 and 435.7 cm^{-1} in an ^{40}Ar environment; the highest-frequency band had three components, assigned to different matrix sites. The intensities of these new absorptions grew proportionally on annealing the sample at about 18 K, and the absorber was found to be stable in our experiments at temperatures below about 27 K. A similar set of new absorptions was obtained in photolysed and annealed DF/^{40}Ar matrixes, the positions now being 1,466.3, 513.0 and 435.3 cm^{-1}. In HF/^{36}Ar samples, the three absorptions shifted to higher frequencies, these shifts being approximately +2, +2 and +7 cm^{-1} from the values given above for HF in ^{40}Ar matrix.

The infrared absorption bands obtained by photolysis and annealing of HF/^{40}Ar, HF/^{36}Ar and DF/^{40}Ar matrixes are shown in Fig. 1. The proportional growth of the three new bands on annealing the sample at different temperatures, as well as their synchronous decrease on ultraviolet irradiation (see below) prove that they belong to the same species. We emphasize that the three infrared absorptions under discussion are completely absent in photolysed and annealed matrices of 'pure' Ar—containing only minor amounts of normal impurities like O_2, N_2, CO_2 and H_2O—showing the participation of F atoms in the absorbing species. Based on deuteration shifts, the two highest-frequency absorptions are predominantly due to hydrogen atom motion. The positions of these absorptions are obviously too low to be due to H–F, H–O, H–N or H–C bonds. The van der Waals complexation of Ar atoms to molecules typically results in vibrational shifts of a few wavenumbers; the greatest shift observed to date (62 cm^{-1}, ~ 4%) being due to an exceptionally strong interaction between Ar and BeO (refs 21, 22). Strong van der Waals interactions between Ar and CuX or AgX (X = F, Cl, Br) have recently been observed[23,24]. Furthermore, the 7.2-cm^{-1} shift of the lowest-wavenumber band on $^{40}Ar \rightarrow {}^{36}Ar$ isotopic substitution shows the presence of Ar chemically bound to a heavier element, which, based on elementary vibrational treatment, is most probably fluorine. On this analysis we assign the three absorptions that we observe to ν(H–Ar), δ(H–Ar–F) and ν(Ar–F) of HArF, isolated in solid Ar. (Here δ indicates a bending vibration.)

HArF photobleaches under ultraviolet irradiation, in a similar fashion to the previously characterized Kr- or Xe-containing molecules[14–17]. The threshold for photodecomposition of HArF is in the region of 350–400 nm. The infrared absorptions of HArF decrease at temperatures above 27 K, when the different photoproducts start to move throughout the matrix; this motion is particularly indicated by the formation of O_3, HOO and FOO. We believe that the mobilization of individual atoms originating from photodissociated HF and matrix impurities is responsible for the decrease of HArF at temperatures above 27 K in solid Ar, due to secondary reactions. Owing to the presence of these thermally activated secondary reactions, the question of the intrinsic thermal stability of HArF in solid Ar remains unanswered for the time being.

The characteristic triplet structure of ν(H–Ar) appears in DF samples, with a maximum at about 1,466.3 cm^{-1}, resulting in a relative deuteration shift (that is, $\nu(H-Ar)/\nu(D-Ar)$ of 1.343. It is worth comparing this value with the deuteration shifts obtained for similar Xe- and Kr-containing hydrides[14–16]. For the strongly bound Xe compounds HXeCN and HXeCl, the shifts are 1.382 and 1.376, respectively. On the other hand, the corresponding numbers for the weakly bound compounds HXeI and HXeSH are 1.336 and 1.343, respectively. The changes in the deuteration shifts display the effect of increasing anharmonicity with the weakening bond between hydrogen and the noble gas. The shift of HArF in Ar is close to the value found for the more weakly bound hydrides containing heavier noble gases.

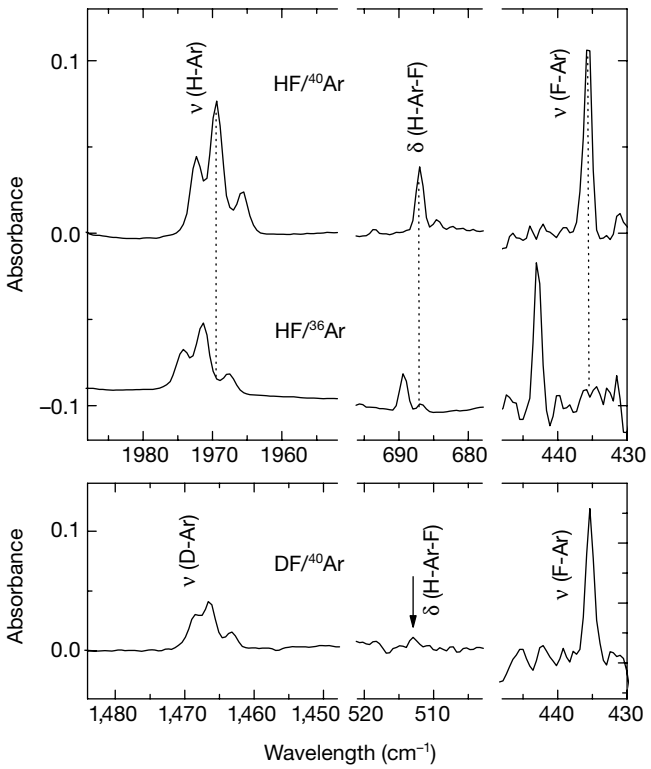

Figure 1 The infrared absorptions of HArF in solid Ar at 7.5 K. This figure shows the effect of $^{40}Ar/^{36}Ar$ and H/D isotopic substitutions. The increased noise in the low-frequency region is due to the low sensitivity of the detector in this region. Note the different scales in the plot. The spectra were recorded at 1 cm^{-1} resolution on a Nicolet 60 SX Fourier-transform infrared (FTIR) spectrometer.

We used molecular-orbital calculations to investigate the molecular properties of HArF: perturbation-theory (MP2) and coupled-cluster (CCSD(T)) calculations were performed using the 'aug-cc-pC5Z' and 'aug-cc-pVTZ' basis sets. All the approaches that we used indicate that the molecule is linear; the CCSD(T)/aug-cc-pV5Z computations yielded H–Ar and Ar–F bond distances of 133 and 197 pm, respectively. The NBO (natural bond orbital) charge distribution obtained at the MP2/aug-cc-pVTZ level of theory indicates a strong ionic character of the molecule, with a positive partial charge on argon (+0.54) and a negative partial charge on fluorine (–0.76). The calculated dipole moment at the CCSD(T)/aug-cc-pV5Z level is 6.51 D. In analogy to the other noble-gas hydrides[14–16] this is an indication of the strong $(HAr)^+F^-$ charge transfer in the HArF electronic structure. This shows that HArF differs completely from the predicted salts containing the strongly bound $(ArF)^+$ unit[9,10]. In order to get an idea of the relative proportions of ionic and covalent contributions in the bonding of HArF, we compare the computed bond lengths and experimental frequencies with published data. The gas-phase harmonic frequency of HAr^+ is 2,710.9 cm^{-1} and the bond distance 128 pm (ref. 25); comparison with the corresponding values for HArF indicates that the complete ionic limit $(HAr)^+F^-$ is not dominating in the molecule. On the other hand, for Ar^+F^- in the $^2\Sigma^+$ state the calculated bond length is 240 pm and the vibrational frequency is 394 cm^{-1} (ref. 26), and the observed frequency in a neon matrix is 415.5 cm^{-1}(ref. 27). These values differ from the present values for HArF—197 pm and 435.7 cm^{-1}—and suggest the presence of covalent contribution in the bonding. Furthermore, the bond length and vibrational frequency of $(ArF)^+$ (163.7 pm and 750 cm^{-1})[10] differ greatly from the corresponding values for HArF.

At the CCSD(T)/aug-cc-pV5Z level, the HArF molecule is 5.87 eV higher in energy than the Ar + HF configuration. The calculated minimum dissociation barrier is along the H–Ar stretching coordinate, and its value is about 0.35 eV. The bending coordinate is connected to a much higher barrier than is the H–Ar stretching, and (according to our computations) it is above 1 eV for HArF. In addition, solvation of a strong dipole in a dielectric host probably provides further stabilization of HArF with respect to its dissociation limit, but this effect is not expected to be a determining factor in the existence of HArF. We note here that our computations refer to the free molecule.

The experimental and computational results for HArF (^{40}Ar and ^{36}Ar) and DArF are compared in Table 1. The CCSD(T)/aug-cc-pVQZ calculations predict the following three vibrations for HArF: Ar–H stretching (2,097 cm^{-1}), Ar–H bending (729 cm^{-1}), and Ar–F stretching (480 cm^{-1}). These vibrational frequencies differ only nominally from those obtained with the smaller VTZ basis. The lower-level MP2/aug-cc-pVTZ calculations give similar results to the CCSD(T) calculations except for the Ar—H stretch, which is now at 2,313 cm^{-1}. The experimental and calculated infrared intensities are very similar, and the calculations predict a considerable intensity decrease for the bending mode on deuteration. For the Kr- and Xe-containing molecules, the hydrogen/noble-gas stretching mode has been noted to be highly anharmonic[14]. Therefore, anharmonic corrections were derived for HArF from the MP2-calculations[28]. Indeed, at the MP2/aug-cc-pVTZ level the anharmonic effect is about 210 cm^{-1} for the Ar–H stretching vibration. For the bending, and the heavy-atom stretching, modes the corrections are smaller, 36 and 8 cm^{-1}, respectively. When the anharmonicity is accounted for, the agreement between the calculated and experimental wavenumbers improves considerably.

The ^{36}Ar–^{40}Ar shift is especially sensitive to the nature of the Ar–F bond; the calculated shift is practically the same as that experimentally observed. We note that our determination of the stretching frequency of the Ar–F bond is clear evidence for the existence of that bond; to our knowledge, this is the first infrared determination of the noble-gas/heavy-atom stretching frequency in the family of noble-gas-containing hydrides. □

Table 1 Experimental and calculated vibrations of HArF

	ν (Ar–H) (cm^{-1})	δ (H–Ar–F) (cm^{-1})	ν (Ar–F) (cm^{-1})
H–^{40}Ar–F			
Experimental	1,969.5*	687.0	435.7
MP2/aug-cc-pVTZ (harm.)	2,313	749	482
MP2/aug-cc-pVTZ (anharm.)	2,103	713	474
CCSD(T)/aug-cc-pVTZ (harm.)	2,053	725	474
CCSD(T)/aug-cc-pVQZ (harm.)	2,097	729	480
D–^{40}Ar–F			
Experimental	1,466.3*	513.0	435.3
CCSD(T)/aug-cc-pVQZ (harm.)	1,500	538	479
H–^{36}Ar–F			
Experimental	1,971.3*	689.3	442.9
CCSD(T)/aug-cc-pVQZ (harm.)	2,100	731	488

*The strongest component of the site-split absorption.

Received 6 April; accepted 19 June 2000.

1. Pauling, L. The formulas of antimonic acid and the antimonates. *J. Am. Chem. Soc.* **55,** 1895–1900 (1933).
2. Bartlett, N. Xenon hexafluoroplatinate(V) $Xe^+[PtF_6]^-$. *Proc. Chem. Soc.* 218 (1962).
3. Graham, L., Graudejus, O., Jha, N., K. & Bartlett, N. Concerning the nature of $XePtF_6$. *Coord. Chem. Rev.* **197,** 321–334 (2000).
4. Holloway, J. H. & Hope, E. G. Recent advances in noble-gas chemistry. *Adv. Inorg. Chem.* **46,** 51–100 (1999).
5. Nelson, L. Y. & Pimentel, G. C. Infrared detection of xenon dichloride. *Inorg. Chem.* **6,** 1758–1759 (1967).
6. Turner, J. J. & Pimentel, G. C. Krypton fluoride: preparation by the matrix isolation technique. *Science* **140,** 974–975 (1963).
7. Bondybey, V. E. *Matrix Isolation Search for Transient Species.* Thesis, Univ. California, Berkeley (1971).
8. Stein, L. Removal of xenon and radon from contaminated atmospheres with dioxygenyl hexafluoroantimonate, O_2SbF_6. *Nature* **243,** 30–32 (1973).
9. Frenking, G. & Cremer, D. The chemistry of the noble gas elements helium, neon and argon. Facts and theoretical predictions. *Struct. Bonding* **73,** 17–95 (1990).
10. Frenking, G., Koch, W., Cremer, D., Gauss, J. & Liebman, J. F. Neon and argon bonding in first-row cations NeX^+ and ArX^+ (X = Li-Ne). *J. Phys. Chem.* **93,** 3410–3418 (1989).
11. Pettersson, M., Lundell, J. & Räsänen, M. Neutral rare gas containing charge-transfer molecules in solid matrices I: HXeCl, HXeBr, HXeI and HKrCl in Kr and Xe. *J. Chem. Phys.* **102,** 6423–6431 (1995).
12. Runeberg, N., Pettersson, M. Khriachtchev, L., Lundell, J. & Räsänen, M. A theoretical study of HArF: an observed neutral argon compound. *J. Chem. Phys.* (submitted).
13. Wong, M. W. Prediction of a metastable heölium compound: H He F. *J. Am. Chem. Soc.* **122,** 6289–6290 (2000).
14. Pettersson, M., Lundell, J. & Räsänen, M. New rare-gas-containing neutral molecules. *Eur. J. Inorg. Chem.* 729–737 (1999).
15. Pettersson, M., Khriachtchev, L., Lundell, J. & Räsänen, M. A chemical compound formed from water and xenon: HXeOH. *J. Am. Chem. Soc.* **121,** 11904–11905 (1999).
16. Pettersson, M., Khriachtchev, L., Lundell, J., Jolkkonen, S. & Räsänen, M. Photochemistry of HNCO in solid xenon: Photoinduced and thermally activated formation of HXeNCO. *J. Phys. Chem. A* **104,** 3579–3583 (2000).
17. Pettersson, M., Nieminen, J., Khriachtchev, L. & Räsänen, M. The mechanism of formation and IR-induced decomposition of HXeI in solid Xe. *J. Chem. Phys.* **107,** 8423–8431 (1997).
18. Lorenz, M., Räsänen, M. & Bondybey, V. E. Neutral xenon hydrides in solid neon and their intrinsic stability. *J. Phys. Chem. A* **104,** 3770–3774 (2000).
19. Hunt, R. D. & Andrews, L. Photolysis of hydrogen fluoride in solid argon. Matrix infrared spectra of $(HF)_2$, (HF)(DF), and $(DF)_2$. *J. Chem. Phys.* **82,** 4442–4448 (1985).
20. Khriachtchev, L., Pettersson, M. & Räsänen, M. On self-limitation of UV photolysis in rare-gas solids and some of its consequences for matrix studies. *Chem. Phys. Lett.* **288,** 727–733 (1998).
21. Thompson, C. A. & Andrews, L. Noble gas complexes with BeO: infrared spectra of Ng-BeO (Ng = Ar, Kr, Xe). *J. Am. Chem. Soc.* **116,** 423–424 (1994).
22. Frenking, G., Koch, W., Gauss, J. & Cremer, D. Stabilities and nature of the attractive interactions in HeBeO, NeBeO, and ArBeO and a comparison with analogues NGLiF, NGBN, and NGLiH (NG = He, Ar). A theoretical investigation. *J. Am. Chem. Soc.* **110,** 8007–8016 (1988).
23. Evans, C. J. & Gerry, M. C. L. Noble gas-metal chemical bonding? The microwave spectra, structures, and hyperfine constants of Ar-CuX (X = F, Cl, Br). *J. Chem. Phys.* **112,** 9363–9374 (2000).
24. Evans, C. J. & Gerry, M. C. L. The microwave spectra and structures of Ar-AgX (X = F, Cl, Br). *J. Chem. Phys.* **112,** 1321–1329 (2000).
25. Johns, J. W. C. Spectra of the protonated rare gases. *J. Mol. Spectrosc.* **106,** 124–133 (1984).
26. Dunning, T. H. Jr & Hay, P. J. The covalent and ionic states of the rare gas monofluorides. *J. Chem. Phys.* **69,** 134–149 (1978).
27. Bressler, C., Lawrence, W. G. & Schwentner, N. Spectroscopy of argon fluoride and krypton fluoride exciplexes in rare gas matrices. *J. Chem. Phys.* **105,** 10178–10188 (1996).
28. Chaban, G. M., Jung, J. O. & Gerber, R. B. Ab initio calculations of anharmonic vibrational states of polyatomic systems: Electronic structure combined with vibrational self-consistent field. *J. Chem. Phys.* **111,** 1823–1829 (1999).

Acknowledgements

We thank P. Pyykkö for discussions. This work was supported by The Academy of Finland.

Correspondence and requests for materials should be addressed to M.R. (e-mail: markku.rasanen@helsinki.fi).